RCNP-Th/00032

Abelian Monopole and Center Vortex Views at the Multi-Instanton Gas

M. Fukushima [†] [‡], **E.–M. Ilgenfritz** [§] **and H. Toki** [**]

Research Center for Nuclear Physics (RCNP), Osaka University, Mihogaoka 10-1, Ibaraki, Osaka 567-0047, Japan

(February 1, 2008)

We consider full non-Abelian, Abelian and center projected lattice field configurations built up from random instanton gas configurations in the continuum. We study the instanton contribution to the $\bar{Q}Q$ force with respect to (*i*) instanton density dependence, (*ii*) Casimir scaling and (*iii*) whether various versions of Abelian dominance hold. We check that the dilute gas formulation for the interaction potential gives an reliable approximation only for densities small compared to the phenomenological value. We find that Casimir scaling does not hold, confirming earlier statements in the literature. We show that the lattice used to discretize the instanton gas configurations has to be sufficiently coarse ($a \approx 2\bar{\rho}$ compared with the instanton size $\bar{\rho}$) such that maximal Abelian gauge projection and center projection as well as the monopole gas contribution to the $\bar{Q}Q$ force reproduce the non-Abelian instanton-mediated force in the intermediate range of linear quasi-confinement. We demonstrate that monopole clustering also depends critically on the discretization scale confirming earlier findings based on monopole blocking.

Key Word: Instantons, monopoles, vortices, confinement

PACS number(s): 12.38.Aw,11.15.Ha

[†]E-mail address: masa@rcnp.osaka-u.ac.jp

[‡]present address: Japan Atomic Energy Research Institute, Ibaraki 319-1195, Japan

[§]E-mail address: ilgen@rcnp.osaka-u.ac.jp

[**]E-mail address: toki@rcnp.osaka-u.ac.jp

I. INTRODUCTION

A few years ago, a RCNP group including two of the present authors [1–3], has started to systematically study the properties of instanton systems with respect to confinement by using multi-instanton simulations. The instanton is a quasi-pointlike topological object in Euclidean space-time and, being selfdual, satisfies the Yang-Mills field equations [4]. Mixed instanton-antiinstanton configurations [5] (gas or liquid) only locally are approximate solutions, but they offer the attractive possibility to solve, in a semiclassical-like fashion, the $U_A(1)$ problem (explain the large η' mass) [6] and to explain chiral symmetry breaking [7,8]. (See Ref. [9] for a recent review.) One main focus of our previous work on instantons, neglected by others, was to explore under which circumstances a dense, however random instanton system could provide confinement. In the beginning [1] it has been pointed out that the monopoles induced in the instanton system and detected by Abelian projection have the clustering property held necessary for confinement. As for the $\bar{Q}Q$ force itself, in Ref. [2,3] quantitatively the conclusion has been reached, after some refinements, that with the widely accepted density of 1 fm^{-4} of instantons plus antiinstantons and an average instanton size of $\bar{\rho} = 0.4$ fm, only 40 % of the static $\bar{Q}Q$ force could be reproduced at distances around $R \approx 1$ fm.

This result was achieved using an instanton size distribution based on the idea of freezing of the strong coupling constant at large distance. This assumption leads to a dimensionally dictated behavior of the size distribution like $dn(\rho)/d\rho \propto \rho^{-5}$ in the infrared. One should remember that the main parameter of any such model, the instanton density and the instanton size distribution are phenomenological input, beyond justification coming from a truly semiclassical approximation. The latter is available only for a single instanton [10], however afflicted with the famous infrared divergence.

Phenomenologically, in the instanton liquid model instantons are occupying Euclidean space with a density of $n = N/V = 1$ fm^{-4}, and with an average radius $\bar{\rho} = 1/3$ fm one gets a packing fraction $f = n\ \bar{\rho}^4 \approx (1/3)^4$. For our purposes we fix only an average instanton radius $\bar{\rho} = 0.4$ fm. We study the influence of the instanton density, considering 1 fm^{-4} as the "physical" value. This leaves some room for the choice of the size distribution.

Lattice search for instantons is *the method of choice* to obtain these quantities and the size distribution relying on first principles. As for pure gluodynamics, *only* lattice studies are at hand presently to quantify the instanton structure of the vacuum. Over the last years the results have not much converged (compare the recent conference reports Ref. [11–13]). Different groups roughly agree on the size of instantons within a factor of two, e.g. $\bar{\rho} = 0.3...0.6$ fm for $SU(3)$. There is no agreement at all concerning the density N/V which is strongly dependent on the procedure to remove size $O(a)$ vacuum fluctuations (cooling, smoothing etc.) and technical parameters (cooling steps, cooling radius etc.)*. As a tendency, lattice studies give higher density and larger

*Sometimes the density $N/V = 1$ fm^{-4} is used as a criterium to stop cooling, in this way

instantons than phenomenologically assumed. It is fair to say that only the topological susceptibility, $\chi_{\rm top}^{\frac{1}{4}}/\sqrt{\sigma} = 0.45(3)$ for $SU(3)$ and $0.50(2)$ for $SU(2)$, and the average instanton size are supported by lattice studies. The instanton size distribution is much more delicate to assess. We will comment on that later.

This paper is dedicated to a critical reappraisal of the instanton model to describe, besides other features of the Yang-Mills vacuum, its confinement property, and we shall clearly point out the deficits of this model. Although seemingly insufficient in quantitative respect, it might be interesting to see to what extent the contribution of instantons to the confining force depends on the ρ distribution. Also the question whether the instanton generated $\bar{Q}Q$ force can be reproduced in accordance to Abelian, monopole or vortex dominance needs some clarification. One has to answer the question at *which scale* the model can be replaced by an effectively Abelian model with condensing Abelian defects. Monopole and $Z(N)$ vortex mechanisms are presently the leading candidates for an effective infrared description comprising confinement. We shall see that these descriptions are applicable to the instanton mediated force as well. This is expected, corroborating earlier work [14] and the widely-studied interrelation between instantons and monopoles [15,16] and the newer studies concerning the interplay of instantons and vortices [17,18], respectively.

Said in another way, what we want to clarify is the complementarity between the explicit semiclassical-like description in terms of continuous instanton fields on one hand and the monopole and vortex aspects on the other. The latter degrees of freedom seem to become physically dominant in the infrared. This is the place where, for our purposes, the lattice discretization appears: it is an infrared matching scale between the instanton picture and the gauge singularities which become manifest in the result of gauge fixing and Abelian projection. If the discretization scale is chosen too small, monopole and vortex degrees of freedom can be identified as well. However, a complementary description of the instanton mediated force can be achieved only if the matching scale is somewhere between the size of and the distance between instantons.

For the sake of clarity we stress that this paper is *not a lattice* study. The lattice is employed here only to enable the necessary coarse-graining of a continuum model. In a lattice gauge theory investigation the rôle of the discretization scale a would be completely different. There a is an ultraviolet cut-off which permits, at the cost of a running bare lattice coupling $\beta \propto 1/g^2$, not to deal *explicitly* with fluctuations of smaller and smaller wave lengths. In this case, the requirement of scale invariance in the limit $a\Lambda \propto \exp\left(-\frac{6}{11}\frac{\pi^2}{N_c}\beta\right) \to 0$ is indeed crucial and must be confirmed for any dimensionful quantity to be physical. Instantons can be found which are stochastically generated within the sample of fields. Being lumps of gauge invariant topological density they are of immediate physical importance. As mentioned above, their average size is relatively well-defined, independently of the lattice scale a (for suitable methods of suppressing the shortest fluctuations living on the lattice). For the confining Abelian defects the situation is somewhat different. They are identified by gauge fixing (which is practically

---

specifying the remaining instanton characteristics.

performed on the lattice of scale a), and the scale invariance of the corresponding density, of the distribution of length or area etc. are controversial. Moreover, it is generally agreed that in order make these defects condensing they have to be defined with some extension (blocked monopoles or thick vortices), a scale which becomes decoupled, in the continuum limit, from the lattice scale a. As far as instantons are discussed as a possible microscopic mechanism to induce Abelian defects, finding the correct matching scale is tantamount to define this extension.

There have been also statements in the literature [19] criticizing the instanton contribution for violating Casimir scaling of the $\bar{Q}Q$ force. While this feature of the non-perturbative force at intermediate distances [20] is largely not understood within Yang-Mills theory and continues to pose a problem for other models of confinement, we want to make clear to what extent this criticism is justified in the case of instanton based models. Finally, many discussions on the instanton generated $\bar{Q}Q$ force are based on a dilute gas formula worked out by Callan, Dashen and Gross [21]. Therefore it is of interest to demonstrate under which circumstances the result of multi-instanton simulations deviates from the one-instanton approximations made in Ref. [21]. In the physical range of packings the effect of different instantons on the Wilson loop is not expected to factorize anymore.

We believe that this study contains some lessons for other attempts of an explicit modeling of the QCD vacuum. The observed scale sensitivity of the monopole or center vortex description seems to be a more general feature of the complementarity between semiclassical continuum models for non-perturbative vacuum structure and condensing defects. It should be remembered that the concept of Abelian and monopole dominance had been introduced as a property of gauge fields in the infrared [22–27], not necessarily on the lattice. Practically, however, all evidence comes from doing the gauge fixing and Abelian projection on the lattice for gauge fields generated by lattice simulation. In the present work the instanton model continuum configurations will be discretized with the purpose to perform the same steps following [25,26] for the monopole part and [28–30] for the vortex part of the heavy quark force. Explicitly calculating these contributions, it turns out that the discretization scale a is an influential *infrared* coarse-graining parameter and must be chosen in correspondence to the typical size and density of the disordering continuum non-perturbative configurations forming the vacuum. This is what our instanton model clearly illustrates.

In section 2 we describe how the lattice discretization of continuum instanton-antiinstanton configurations is done. In section 3 we demonstrate that the one-instanton description of the $\bar{Q}Q$ force breaks down already in moderately dense instanton gases. In the same section we study to what extent the forces for quarks and adjoint charges deviate from Casimir scaling. Section 4 deals with the question how coarse-graining the lattice has to be chosen such that Abelian projection, the monopole gas and the center projection are able to reproduce the non-Abelian instanton-mediated force. In section 5 we show, for the case of monopoles, that this necessary blocking corresponds to the percolation property held necessary for confinement. We summarize and conclude in section 6.

II. CONTINUUM MULTI-INSTANTON CONFIGURATIONS AND THEIR DISCRETIZATION

We base our studies of the $\bar{Q}Q$ force and possible complementary descriptions in terms of monopoles and center vortices on a model which comprises the Yang-Mills vacuum as an ensemble of random collections of instantons and antiinstantons. The interaction is partly taken into account in the size distribution given below.

In order to fix the scale of our continuum model, we choose an average instanton size $\overline{\rho} = 0.4$ fm. The average size is most solidly defined by the profile of the topological density after a few cooling steps. Our choice realistically applies to $SU(2)$ Yang-Mills theory. Unless stated otherwise (when we study the density dependence of the instanton mediated force in section 3) the density is chosen $N/V = (N_I + N_{\bar{I}})/V = 1$ fm^{-4} with the packing fraction $f = \bar{\rho}^4 \frac{N}{V} = 0.0256$.

We adopt the sum ansatz [32]

$$A_\mu(x) = \sum_k A^I_\mu(x; z_k, \rho_k, O_k) + \sum_{\bar{k}} A^{\bar{I}}_\mu(x; z_{\bar{k}}, \rho_{\bar{k}}, O_{\bar{k}}), \tag{1}$$

in terms of instanton and anti-instanton solutions in the singular gauge where an instanton is written as

$$A^I_\mu(x; z, \rho, O) = \frac{2i\ O^{ab}\bar{\eta}^{b\mu\nu}(x-z)_\nu \rho^2}{(x-z)^2\ [(x-z)^2 + \rho^2\ ]} \frac{\tau^a}{2}. \tag{2}$$

Here ρ and z denote the instanton size and the space-time position of the instanton center, respectively. The instanton solution can be rotated in color space by the color orientation matrix O. The 't Hooft symbol $\bar{\eta}^{b\mu\nu}$ is defined as $\bar{\eta}^{b\mu\nu} \equiv \varepsilon^{b\mu\nu}(1 - \delta^{4\mu}\delta^{4\nu}) - \delta^{b\mu}\delta^{4\nu} + \delta^{b\nu}\delta^{4\mu}$. The anti-selfdual solution $A^{\bar{I}}_\mu$ is obtained replacing $\bar{\eta}^{b\mu\nu}$ by $\eta^{b\mu\nu} \equiv (-1)^{\delta^{\mu 4}+\delta^{\nu 4}}\bar{\eta}^{b\mu\nu}$. The instanton solutions have several gluonic collective modes related to variations of parameters like size and position (five collective degrees of freedom). For pure $SU(2)$ gauge theory, the color orientation matrix is characterized by 3 parameters (the Euler angles). For N_c colors the number of collective parameters (and gluonic zero modes) generalizes to $4N_c$.

Actually, we generate the ensemble of instantons and anti-instantons by randomly placing z_k in a 4-dimensional Euclidean continuum box. The (adjoint) color orientations O_k are taken randomly with the Haar measure, and the instanton sizes ρ_k are sampled according to the following size distribution :

$$\frac{dn(\rho)}{d\rho} = \alpha\ \rho^{b-5} \exp(-\beta\rho^2/\overline{\rho^2}) \tag{3}$$

with $b = 11N_c/3$. Here α and β are fixed by normalizing to the space-time density as $\int_0^\infty dn(\rho) = N/V$ and the average size $\int_0^\infty \rho\ dn(\rho) = \bar{\rho}\ N/V$. In the explicit configurations, the instanton number N_I is taken equal to that of the antiinstantons $N_{\bar{I}}$.

This form of the size distribution was originally established in a mean-field treatment of color-averaged interactions [32]. Averaged over orientations, the interaction of equal-sign and opposite-sign pairs is repulsive, $S_{\rm int} \propto \rho_1^2\ \rho_2^2$. In the mean-field approximation for the one-instanton distribution, this results in a suppression exponentially in ρ^2.

As for the lattice evidence for such an instanton size distribution we refer to the systematic problems mentioned in the Introduction. One should keep in mind that instanton finding algorithms depend on cooling or smoothing. Huge instantons distinguished by a very weak field strength could become washed out within the first steps of cooling [36] together with the noise. Smith and Teper [33] have reported an instanton ρ distribution from quenched $SU(3)$ lattice ensembles resembling an exponential cutoff at large ρ. The size distribution found by Hasenfratz and Nieter [34] has been interpreted by Shuryak [35] in an exponentially suppressed parameterization in terms of a dual Higgs mechanism. There are also other warnings, motivated by the wealth of semiclassical configurations known today [37], not too early to take for granted the size cut-off as seen in the lattice studies of Refs. [33,34].

Very recently, in Ref. [38], a distribution like (3) has been demonstrated to emerge, in dimension $d > 2$, from a very general model of soft (inflatable) spheres with excluded-volume interaction which inherits from QCD not more than the semiclassical perturbative instanton fugacity proportional to ρ^{b-5}. In the grand canonical Monte Carlo simulation of this system the ρ dependent fugacity has been used in conjunction with the excluded-volume constraint.

Because the instantons are randomly placed inside the box, it might be interesting to know how frequently instantons are strongly overlapping, which we define by $\rho_1\ \rho_2/\Delta_{12}^2 > 1$ (where Δ_{12} is the Euclidean distance). For the size distribution (3) and the physical density of 1 fm^{-4}, the number $N_<$ of strongly overlapping pairs (including all possible pairings between instantons and antiinstantons) relative to the total number $N = N_+ + N_-$ of instantons and antiinstantons amounts to $N_</N = 0.072$. This fraction actually depends on the width of the size distribution. For instance, for a sharp distribution $\frac{dn(\rho)}{d\rho} \propto \delta(\rho - \bar\rho)$ one would find, with the same density and $\bar\rho$, a smaller fraction $N_</N = 0.056$ of closely packed pairs. We are aware of the problem that the linear superposition ansatz should be replaced by some better ansatz (ratio ansatz) for close instanton-instanton pairs and by the streamline ansatz for instanton-antiinstanton pairs at high densities. For the observed percentage of close pairs in the physical range of densities, we have neglected this potential complication. This improvement would become more important with an algebraically falling size distribution.

In our actual calculation, we cover the random multi-instanton configuration by a lattice similar to Ref. [3]. For the calculation of the fully non-Abelian force the discretization actually would not be necessary. In fact, we choose a sufficiently fine lattice spacing of $a = 0.05$ fm (this should be compared with the average instanton size of $\bar\rho = 0.4$ fm). For this case (of the finest lattice) the link variables are given simply as $U_\mu(x) = \exp[iaA_\mu(x + \frac{1}{2}\hat\mu a)]$ using the gluon field of the multi-instanton system on the mid-point of the link $l = \{x, \mu\}$. In connection with Abelian gauges and Abelian projections, we will apply a coarser discretization scale. Then the $SU(2)$ link variables

are constructed by integrating the vector potential defined on the continuum space as

$$U_l = U_\mu(x) \;=\; \mathrm{P}\;\exp\Big[\int_x^{x+\hat{\mu}a} dx'_\mu A_\mu(x')\Big]$$
$$= \mathrm{P}\;\prod_{j=1}^{l}\exp\Big[\;\tilde{a}\;A_\mu(x+(j-\frac{1}{2})\;\hat{\mu}\tilde{a})\;\Big]\;. \qquad (4)$$

Here, the path from x to $x+\hat{\mu}a$ has been subdivided into smaller segments with step size of $\tilde{a}=a/l$, and the above path ordered exponential has been calculated as a product over finer links defined on these segments. Actually, we take $\tilde{a}=0.05$ fm as the segment size. This construction becomes increasingly important when the discretization scale of the lattice gets comparable with or larger than the average instanton size.

Periodicity of the lattice gauge field configurations has been enforced by placing the 4-dimensional Euclidean box of size $V=(4.8\ \mathrm{fm})^4$ (to be covered by the lattice) into a bigger box. The 3-dimensional boundary in each of the eight directions is extended to a 4-dimensional slab of thickness 1.2 fm continuing the basic box. In each of these slabs copies (phantom instantons) are placed of instantons which are near to the opposite boundary. These are also included into the sum (1) representing the continuum vector potential. Then, along the links restricted to the basic box the above construction is performed.

III. THE $\bar{Q}Q$ POTENTIAL FROM THE RANDOM INSTANTON LIQUID AND THE DILUTE GAS LIMIT

The effect of instantons on the heavy quark potential has been first discussed in Ref. [21] by using the dilute gas approximation. There a formula has been derived according to which the static potential could be written as

$$V(R)=2\int d\rho\frac{dn(\rho)}{d\rho}\;\rho^3\;W\left(\frac{R}{\rho}\right), \qquad (5)$$

where $dn(\rho)/d\rho$ is the respective instanton size distribution and the factor two refers to instantons plus antiinstantons. Here, a dimensionless potential $W(R/\rho)$ ($R=|\vec{r}|$) is defined by integration over the instanton position $\vec{x}$

$$W\left(\frac{R}{\rho}\right)=-\frac{1}{2\rho^3}\int d^3x\;\mathrm{tr}\;\;[\;U(\vec{r}-\vec{x})U^\dagger(-\vec{x})-1\;]\;. \qquad (6)$$

The fundamental static charges ($j=\frac{1}{2}$) are represented by static trajectories positioned at $\vec{0}$ and $\vec{r}$ in 3-space (with $R=\mid\vec{r}\mid$). The color matrix $U(\vec{r}-\vec{x})$ represents the path ordered exponential along one of the infinite trajectories traversing the instanton and is given as $U(\vec{r}-\vec{x})=\exp[i\;\pi\;\vec{\tau}\cdot(\vec{r}-\vec{x})/\;[\;(\vec{r}-\vec{x})^2+\rho^2\;]^{1/2}]$. It depends only on the instanton size ρ and the shortest distance from the trajectory to the instanton center. Notice that the instanton orientation does not matter. That part of integration is normalized to

unity. Replacing the trace $\frac{1}{2}\mathrm{tr}(U_1\,U_2^\dagger)$ in (6) by the trace in the adjoint representation, $\frac{1}{3}\mathrm{tr}_{\mathrm{ad}}(U_1\,U_2^\dagger) = \frac{1}{3}\left((\mathrm{tr}(U_1\,U_2^\dagger))^2 - 1\right)$ one can extend (5) to the adjoint ($j = 1$) charges. For the comparison in this section we adopt the instanton size distribution in the form of eq. (3) and confront the dilute gas result (5) with multi-instanton simulation results where the same distribution has been used for sampling of the ρ_k's. In this section, the total density N/V is a free parameter.

The potential (for fundamental and adjoint charges) obtained from eq. (5) is simply proportional to the density N/V as shown in Fig. 1 by the solid lines. The data symbols in Fig. 1 denote the results of an uncorrelated multi-instanton simulations. The comparison is made for the instanton densities (a) $N/V = 0.05$ fm^{-4}, (b) $N/V = 0.20$ fm^{-4}, (c) $N/V = 0.60$ fm^{-4}, and (d) $N/V = 1.00$ fm^{-4}. The results of the simulation are based on a statistics of (a) 100, (b) 300, (c) 500, and (d) 1000 configurations respectively. The left panels show the potential between fundamental charges, while the right panels between adjoint charges.

The simulation data have been obtained, using the lattice discretization of the random instanton-antiinstanton configurations as described above, from expectation values of Wilson loops

$$\langle W_{full}(R,T)\rangle = \langle \mathrm{Tr} \prod_{l\in C} U_l\rangle \tag{7}$$

where the contour C is a rectangular closed path of size $R \times T$ on the finest lattice of $a = 0.05$ fm, a spacing almost 10 times smaller than the average instanton size. The non-Abelian potential

$$V(R) = -\frac{1}{a}\ \log \frac{\langle W_{\mathrm{full}}(R,T)\rangle}{\langle W_{\mathrm{full}}(R,T-1)\rangle} \tag{8}$$

has been constructed from the discrete logarithmic time derivative.

We see that eq. (5) is only approximate and applicable only for a system of widely separated uncorrelated instantons and/or antiinstantons. Then the effect of single instantons exponentiates in a Wilson loop at finite temporal extension T. Only at very small distance, where overlapping of instantons can be neglected, simulation and analytical formula agree in the quadratic behavior of the potential.

Already for a moderate density of $N/V = 0.2$ fm^{-4} deviations are remarkable which develop differently with higher density for fundamental and adjoint charges. From the comparison we conclude that the dilute gas formula for fundamental and adjoint charges is valid only up to a density of 0.05 fm^{-4} which corresponds to a packing fraction $f = 1.3\ \times 10^{-3}$. Corrections become visible first at large distances of $R \approx 1.5$ fm. We show this for the density 0.2 fm^{-4} corresponding to a packing fraction $f = 5.2\ \times 10^{-3}$. The resulting potential from the multi-instanton simulation continues to rise where the dilute-gas formula starts already leveling off.

For the comparison of the instanton contributions to the forces between "quark" and "antiquark" in the fundamental and adjoint representation, respectively, it is more

illuminating to consider the derivatives of the potentials shown in Fig. 1. We are interested now in a instanton gas of realistic density and show in Fig. 2 the result of simulations for $N/V = 0.6$ fm^{-4} only, together with the dilute gas result. The ratio between the adjoint and the fundamental charge is < 2 at all distances and is closest to the Casimir ratio, $\frac{9}{4}$ at $R = 0.5$ fm $\approx \bar{\rho}$ where the instanton contribution itself is maximal. The ratio becomes quite small as the distance increases. This tendency is seen for the other densities, too.

In Fig. 3 we show the density dependence of the $\bar{Q}Q$ force at two distances, $R = 0.9$ fm $\approx 2\ \bar{\rho}$ and $R = 1.5$ fm, above (a) for fundamental, below (b) for adjoint charges. It is interesting to see for the smaller distance that both forces rise with the instanton density N/V almost linearly, with a slope compatible with the dilute gas (one-instanton) approximation, up to $N/V \sim 0.6$ fm^{-4}. The forces drop down significantly at higher density, as shown by simulations at $N/V = 1$ fm^{-4}, in the case of fundamental charges relatively to the dilute gas extrapolation, while in the case of adjoint charges even absolutely. A similar behavior is obtained for all $R < 1$ fm. On the other hand, for $R > 1$ fm the behavior is different. We show this for $R \sim 1.5$ fm. The force in the fundamental representation rises almost linearly in the density with a slope exceeding the dilute gas approximation by ≈ 50 %, while the force in the adjoint representation drops already at small density below the dilute gas result.

IV. VARIOUS ABELIAN PROJECTIONS OF MULTI-INSTANTON CONFIGURATIONS

In this section, we want to clarify how concepts like Abelian dominance, monopole dominance, center dominance can be applied to semiclassical-like multi-instanton configurations. We shall compare the fully non-Abelian force discussed in section 2 with the results obtained after standard techniques of gauge fixing and Abelian projection have been applied to the multi-instanton fields and the respective contributions to the static $Q\bar{Q}$ force have been evaluated. Technically, as a coarse-graining device, the continuum configurations are latticized, and the results will depend critically on the lattice spacing compared with the average instanton size.

For this study the periodic Euclidean box of size $V = (4.8\ \text{fm})^4$ is discretized with four different lattice spacings, $a = 0.2$ fm, $a = 0.4$ fm, $a = 0.6$ fm, and $a = 0.8$ fm, corresponding to lattices 24^4, 12^4, 8^4 and 6^4, respectively. In all cases, we have chosen $\tilde{a} = 0.05$ fm as the segment size (integration step) to construct the links (path ordered exponential) of the lattice configuration. How periodicity is enforced has been described in section 2.

First, we consider the maximally Abelian gauge [39] (MAG), which is defined by maximizing the functional

$$R_{MA} = \sum_{x,\mu} \text{tr}\ [U_\mu(x)\ \tau^3\ U_\mu^\dagger(x)\ \tau^3] \tag{9}$$

with $U_\mu(x) = U_\mu^0(x) + i\tau^i U_\mu^i(x)$. In the MA gauge, the $SU(2)$ link variable $U_\mu(x)$ is

decomposed as

$$
\begin{aligned}
& U_\mu(x) = M_\mu(x) u_\mu(x) \\
&= \begin{pmatrix} \sqrt{1- \mid c_\mu(x) \mid^2} & -c_\mu^*(x) \\ c_\mu(x) & \sqrt{1- \mid c_\mu(x) \mid^2} \end{pmatrix} \begin{pmatrix} e^{i\theta_\mu(x)} & 0 \\ 0 & e^{-i\theta_\mu(x)} \end{pmatrix},
\end{aligned} \tag{10}
$$

where the Abelian angle variable $\theta_\mu(x)$ and the non-Abelian variable $c_\mu(x)$ are defined in terms of $U_\mu(x)$ as $\tan\theta_\mu(x) = U_\mu^3(x)/U_\mu^0(x)$, $c_\mu(x)e^{i\theta_\mu(x)} = [-U_\mu^2(x) + iU_\mu^1(x)]$. To clarify the contribution of Abelian components to the static force, we consider the Abelian projection of full non-Abelian link variables U_μ to the Abelian ones u_μ. This is tantamount to replacing, in a Yang-Mills vacuum configuration put into MA gauge, of the $SU(2)$ link variables by $U(1)$ link variables, $U_\mu(x) \to u_\mu(x)$. Before this is done the off-diagonal parts $U_\mu^1(x)$ and $U_\mu^2(x)$ of gluon fields have been minimized by the gauge transformation which has to be found iteratively.

One can further decompose the diagonal gluon component θ_μ into the monopole part θ_μ^{mo} and the photon part θ_μ^{ph}. Using the forward derivative $\partial_\mu f(x) \equiv f(x+\hat{\mu}a) - f(x)$, the 2-form $\theta_{\mu\nu}(x) \equiv \partial_\mu\theta_\nu(x) - \partial_\nu\theta_\mu(x)$ defines the field strength which is separated as follows

$$
\theta_{\mu\nu}(x) = \bar{\theta}_{\mu\nu}(x) + 2\pi n_{\mu\nu}(x) \tag{11}
$$

into a gauge invariant regular field strength $\bar{\theta}_{\mu\nu}(x) \equiv \mathrm{mod}_{2\pi}\theta_{\mu\nu}(x) \in (-\pi, \pi]$ and a Dirac string part $n_{\mu\nu}(x) \in \mathbf{Z}$.

From each part of the field strength the photon part $\theta_\mu^{ph}(x)$ and the monopole part $\theta_\mu^{mo}(x)$ of the $U(1)$ vector potential can be reconstructed, for instance

$$
\theta_\mu^{mo}(x) = 2\pi \sum_{x'} \Box^{-1}(x-x')\partial_\nu n_{\mu\nu}(x'), \tag{12}
$$

using the lattice Coulomb propagator $\Box^{-1} = (\partial_\mu\partial'_\mu)^{-1}$, where ∂'_μ denotes the backward derivative. Then, we can construct the Abelian projected Wilson loop as

$$
\langle W_{abel}(C)\rangle = \langle \exp[i \oint_C \theta_\mu(x)\, dx_\mu]\rangle \tag{13}
$$

which contains, besides of a "photonic" Wilson loop the monopole projected Wilson loop

$$
\langle W_{mon}(C)\rangle = \langle \exp[i \oint_c \theta_\mu^{mo}\, dx_\mu]\rangle \tag{14}
$$

as a uniquely defined factor.

On the other hand, we can also consider the center projection of an instanton configuration. This requires to go through the lattice discretization, too. Then, we use the direct maximal center gauge [29]. This gauge is defined as the gauge which

brings directly the full link variables U_l as close as possible to the center elements $\pm I$ by maximizing

$$R_{MC} = \sum_{x,\mu} [\text{tr } U_\mu(x)]^2. \tag{15}$$

In this gauge the center projection is defined by

$$Z_\mu(x) = \text{sign}[\text{tr } U_\mu(x)]. \tag{16}$$

After the gauge fixing, there remains only a local $Z(2)$ symmetry as $U_\mu(x) \to z(x)z(x+\hat{\mu}a)U_\mu(x)$ with $z(x) \in Z(2)$ Then, we can construct the center projected Wilson loop as

$$\langle W_{center}(C)\rangle = \langle \prod_{l\in C} Z_l \rangle. \tag{17}$$

In Fig. 4, we show the instanton mediated non-perturbative force for the standard density 1 fm^{-4} and fixed average instanton size $\bar{\rho} = 0.4$ fm. Instanton sizes were sampled according to the exponentially damped size distribution (3). The simulation data are based on a statistics of 1000 multiinstanton configurations for each discretization scale.

As shown in Fig. 4(a), for a lattice spacing much smaller than the typical size of instantons, the Abelian force calculated after Abelian projection from (13) does not reproduce the non-Abelian force. Moreover, the Abelian force is practically reproduced after the monopole component of the Abelian field has been removed (by the "photonic" Wilson loops alone). The monopole contribution to the heavy charge force turns out to be smaller by a factor of two. The $Z(2)$ force calculated within the center-projected configurations is completely negligible.

For comparison we show in Fig. 4(b) the same for a coarser lattice of lattice spacing $a = 0.4$ fm $= \bar{\rho}$. In this case, the Abelian force has increased but it is still far from reproducing the non-Abelian force. The center component of the force has become measurable and is comparable with the monopole component which has also increased somewhat.

This trend continues when we consider a even coarser lattice in Fig. 4(c) with $a = 0.6$ fm $= 1.5\bar{\rho}$. In Fig. 4(d) we show the coarsest lattice with $a = 0.8$ fm $= 2\bar{\rho}$. Now the slopes of the potentials calculated in the various projections are in agreement with Abelian, monopole and center dominance, with an ordering of the quasi-string tensions $\sigma_{\text{SU(2)}} > \sigma_{\text{Abelian}} > \sigma_{\text{Z(2)}} \approx \sigma_{\text{mono}}$. Here, of course, the potential can be looked at only at one or two lattice spacings. Therefore the values of the string tension should be considered only as rough estimates.

V. MONOPOLE CURRENT PERCOLATION

The monopole current can be defined using $u_\mu(x)$ following DeGrand and Toussaint [40]. Since the Bianchi identity regarding the Abelian field strength $\bar{\theta}_{\mu\nu}(x)$ is

broken by the decomposition in eq. (11), a monopole current $k_\mu(^*x)$ can be defined on the dual link $\{^*x, \mu\}$ as

$$k_\mu(^*x) \equiv \frac{1}{4\pi}\varepsilon_{\mu\nu\alpha\beta}\partial_\nu\bar{\theta}_{\alpha\beta}(x+\hat{\mu}a) = -\partial_\nu\tilde{n}_{\mu\nu}(^*x) \tag{18}$$

where $\tilde{n}_{\mu\nu}(x) \equiv \frac{1}{2}\varepsilon_{\mu\nu\alpha\beta}n_{\alpha\beta}(x+\hat{\mu}a)$. This current is obviously conserved, $\partial'_\mu k_\mu(^*s) = 0$ which results in closed monopole loops on the 4-dimensional dual lattice. Here, ∂'_μ denotes the backward derivative.

In the previous paper [3], "block-spin" transformations (of type II) have been applied to the monopole currents [41,42] in order to study how the global structure of the monopole loops changes for Abelian projected multi-instanton configurations. For large-scale blocking, leading to monopole currents defined on a very coarse (infrared) lattice, monopole clustering appears, i.e. clusters of big monopole length are seen to form.

Instead of this, in the present study, we consider first the Abelian projection performed on lattices with different lattice spacings. The different lattices would be related, in the sense of [41] by type I block spin transformations. For us, the difference is just in the choice of the discretization scale for our multiinstanton configurations. The histograms have been, however, obtained in independent runs. In the case of Figs. 5 (a) and (b), 2000 multiinstanton configurations have been evaluated, in the case of Figs. 5 (c) and (d) the statistics was 500 configurations each. The Figs. 5 show histograms dN/dl monopole clusters normalized to the average occurrence in one configuration. The integral over lengths, $\int dN(l)$, gives the average number of separate clusters per configuration, while $\int l\ dN(l)$ gives the average total length. When the projection is performed on a lattice with $a << \bar{\rho}$ (in our case $a = \frac{1}{2}\ \bar{\rho}$) the histogram of monopole loops per configuration with respect to their loop length (cluster size) contains only a component of relatively short loops as shown in Fig. 5(a). If the projection is done on a lattice with $a = 2\bar{\rho}$ the histogram Fig. 5(c) has already a component of monopole currents which percolate. One very long monopole cluster of complicated structure appears per configuration with a discretization scale $a = 2\bar{\rho}$, similar to what has been observed previously [3], as shown in Fig. 5(d).

In Fig. 6 we show, in a 3-dimensional cut, the instanton and monopole content of a characteristic configuration at that density. The cross-shaped endcaps of the bars symbolize that the monopole world lines leave (enter) the volume going to (coming from) another timeslice. In MAG, the monopole network (percolating at the coarsest lattice) is wrapping the instantons.

VI. SUMMARY AND CONCLUSIONS

We have studied the static quark potential induced by a random instanton liquid. We have made the present study in the sequel of the previous work [3] where an infrared suppression of the instanton size distribution $dn(\rho) \propto \rho^{-\nu}\ d\rho$ has been assumed. In this paper, we adopt a size distribution as $dn(\rho)/d\rho = \alpha\rho^{b-5}\exp(-\beta\rho^2/\overline{\rho^2})$ (suggested

by lattice instanton searches) adapted to a space-time density of $N/V = 1$ fm^{-4} and an average instanton size $\bar{\rho} = 0.4$ fm. We find that the gross effects do not depend on the detailed form of the size distribution.

First, we have compared the non-Abelian potential inferred from the Wilson loop embedded in the simulated random multi-instanton ensemble with the well-known dilute-gas expression which reduces the potential to the effect of isolated single instantons. We found that the dilute gas expression differs essentially from the simulation results if the density is bigger than $\frac{1}{20}$ of the phenomenological value, due to many instantons interacting with a Wilson loop in a non-exponentiable way. This explains why the quasi-linear part of the $\bar{Q}Q$ force at $R \sim 1 - 1.5$ fm needs to be found from a simulation. We have found that the force between adjoint charges behaves more complicated in the multi-instanton system.

Second, we have investigated the Abelian and center projection of the gauge field configurations built up by random instanton configuration. The gauge fixing and subsequent projection has been performed introducing lattices of different lattice spacing, and we have studied the effect of changing the discretization scale, in particular checking lattice spacings $a = 0.2$, 0.4, 0.6 and 0.8 fm. In the finer lattice case, the monopole contribution to the heavy charge force turns out to be much smaller than the Abelian projected force. The force calculated for the center-projected configurations is completely negligible. With larger and larger discretization scale, Abelian, monopole and center dominance becomes restored, which is almost perfectly illustrated for $a = 2\bar{\rho}$. Then the quasi-linear non-Abelian force can be almost reproduced by the corresponding projected Wilson loops.

We stress this result, although the random instanton liquid model as such does not appear to be a realistic model for the confining aspect of the Yang-Mills vacuum, because this seems to reflect a more general feature to be kept in mind for more sophisticated semiclassical models.

We see that in the multi-instanton liquid, at $a = 2\ \bar{\rho}$, Abelian dominance of the heavy charge force amounts to about 90 %, which is mainly due to the Abelian monopole component. The singular part of the Abelian gauge potential accounts for 80 % of the Abelian force. The center projected force now also describes about 80 % of the non-Abelian one.

We have considered the monopole loop percolation behavior in the random multi-instanton configurations using the same typical lattice spacings. Only after performing the projection with a discretization scale $a > \bar{\rho}$ we could find a percolating component among the monopole currents, represented by one or few clusters of huge loop length per configuration. This parallels the previous observation in Ref. [3] that blocking of monopole currents is necessary to see percolation/condensation happening.

ACKNOWLEDGMENT

E.-M. I. gratefully acknowledges the support by the Ministry of Education, Culture and Science of Japan (Monbu-sho) providing the opportunity to work at RCNP. M. F. is supported by JAERI as a research fellow.

---

[1] M. Fukushima, S. Sasaki, H. Suganuma, A. Tanaka, H. Toki, and D. Diakonov, Phys. Lett. **B 399**, 141 (1997).
[2] M. Fukushima, H. Suganuma, A. Tanaka, H. Toki, and S. Sasaki, Nucl. Phys. Proc. Suppl. **63**, 513 (1998).
[3] M. Fukushima, H. Suganuma, and H. Toki, Phys. Rev. **D 60**, 094504 (1999).
[4] A. A. Belavin, A. M. Polyakov, A. S. Shvarts, and Yu. S. Tyupkin, Phys. Lett. **B 59**, 85 (1975).
[5] C. G. Callan, R. Dashen, and D. J. Gross, Phys. Rev. **D 17**, 2717 (1978), Phys. Rev. **D 19**, 1826 (1979).
[6] G. 't Hooft, Phys. Rev. Lett. **37**, 8 (1976).
[7] D. Diakonov and V. Yu. Petrov, Phys. Lett. **B 147**, 351 (1984); Nucl. Phys. **B 272**, 457 (1986).
[8] E. V. Shuryak, Nucl. Phys. **B 302**, 599 (1988); E. V. Shuryak and J.J.M. Verbaarschot, Nucl. Phys. **B 341**, 1 (1990).
[9] T. Schäfer and E. V. Shuryak, Rev. Mod. Phys. **70**, 323 (1998).
[10] G. 't Hooft, Phys. Rev. **D 14**, 3432 (1976), Erratum-ibid. **D 18**, 2199 (1978).
[11] J. W. Negele, Nucl. Phys. Proc. Suppl. **73**, 92 (1999).
[12] M. Teper, Nucl. Phys. Proc. Suppl. **83**, 146 (2000).
[13] M. Garcia Perez, e-Print Archive: hep-lat/0011026 (plenary talk at Lattice'2000).
[14] H. Suganuma, M. Fukushima, H. Ichie, and A. Tanaka, Nucl. Phys. Proc. Suppl. **65**, 29 (1998).
[15] H. Markum, W. Sakuler, and S. Thurner, Nucl. Phys. Proc. Suppl. **47**, 254 (1996); M. Feurstein, H. Markum, and S. Thurner, Phys. Lett. **B 396**, 203 (1997).
[16] M. Feurstein, E.-M. Ilgenfritz, M. Müller-Preussker, and S. Thurner, Nucl. Phys. **B 511** 421 (1998); E.-M. Ilgenfritz, H. Markum, M. Müller-Preussker, and S. Thurner, Phys. Rev. **D 58**, 094502 (1998); Phys. Rev. **D 61**, 054501 (2000).
[17] O. Jahn, F. Lenz, J. W. Negele, and M. Thies, Nucl. Phys. Proc. Suppl. **83**, 524 (2000).
[18] Ph. de Forcrand and M. Pepe, e-Print Archive: hep-lat/0010093 (talk at Lattice'2000).
[19] V. I. Shevchenko and Yu. A. Simonov, Phys. Rev. Lett. **85**, 1811 (2000); Yu. A. Simonov, JETP Lett. **71**, 127 (2000).
[20] G. S. Bali, Nucl. Phys. Proc. Suppl. **83**, 422 (2000); Phys. Rev. **D 62**, 114503 (2000).
[21] C. G. Callan, R. Dashen, D. J. Gross, F. Wilczek, and A. Zee, Phys. Rev. **D 18**, 4684 (1978).
[22] G. 't Hooft, Nucl. Phys. **B 190**, 455 (1981).
[23] Z. F. Ezawa and A. Iwazaki, Phys. Rev. **D 25**, 2681; Phys. Rev. **D 26**, 631 (1982).
[24] T. Suzuki and I. Yotsuyanagi, Phys. Rev. **D 42**, 4257 (1990).

[25] J. D. Stack, S. D. Neiman, and R. J. Wensley, Phys. Rev. **D 50**, 3399 (1994).
[26] H. Shiba and T. Suzuki, Phys. Lett. **B 333**, 461 (1994).
[27] G. S. Bali, V. Bornyakov, M. Müller-Preussker, and K. Schilling, Phys. Rev. **D 54**, 2863 (1996).
[28] L. Del Debbio, M. Faber, J. Greensite, and S. Olejnik, Phys. Rev. **D 55**, 2298 (1997).
[29] L. Del Debbio, M. Faber, J. Giedt, J. Greensite, and S. Olejnik, Phys. Rev. **D 58**, 094501 (1998).
[30] K. Langfeld, H. Reinhardt, and O.Tennert, Phys. Lett. **B 419**, 317 (1998);
M. Engelhardt, K. Langfeld, H. Reinhardt, and O. Tennert, Phys. Lett. **B 431**, 141 (1998); Phys. Rev. **D 61**, 054504 (2000).
[31] M. Pepe and Ph. de Forcrand, e-Print Archive: hep-lat/0008014.
[32] D. Diakonov and V. Yu. Petrov, Nucl. Phys. **B 245**, 259 (1984).
[33] D. A. Smith and M. J. Teper, Phys. Rev. **D 58**, 014505 (1998).
[34] A. Hasenfratz and C. Nieter, Phys. Lett. **B 439**, 366 (1998).
[35] E. V. Shuryak, e-Print Archive: hep-ph/9909458.
[36] E.-M. Ilgenfritz and S. Thurner, in preparation.
[37] M. Garcia Perez, T. G. Kovacs, and P. van Baal, Phys. Lett. **B 472**, 295 (2000).
[38] G. Münster and Ch. Kamp, Eur. Phys. J. **C 17**, 447 (2000).
[39] A. S. Kronfeld, M. L. Laursen, G. Schierholz, and U. J. Wiese, Phys. Lett. **B 198**, 516 (1987); A. S. Kronfeld, G. Schierholz, and U. J. Wiese, Nucl. Phys. **B 293**, 461 (1987).
[40] T. A. DeGrand and D. Toussaint, Phys. Rev. **D 22**, 2478 (1980).
[41] T. L. Ivanenko, A. V. Pochinsky, and M. I. Polikarpov, Phys. Lett. **B 252**, 631 (1990).
[42] T. Suzuki, Y. Matsubara, S. Ejiri, K. Yamada, and N. Arasaki, Nucl. Phys. Proc. Suppl. **47**, 270 (1996).

VII. FIGURE CAPTION

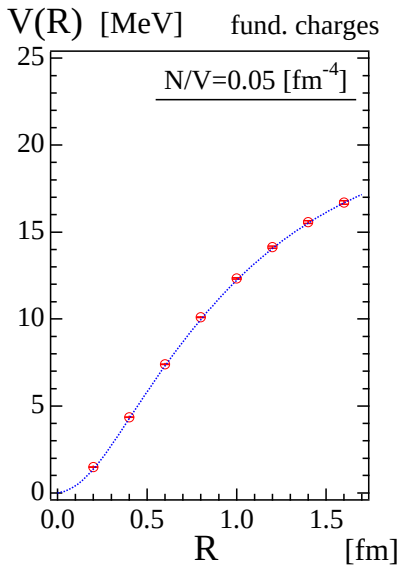

(a-i)

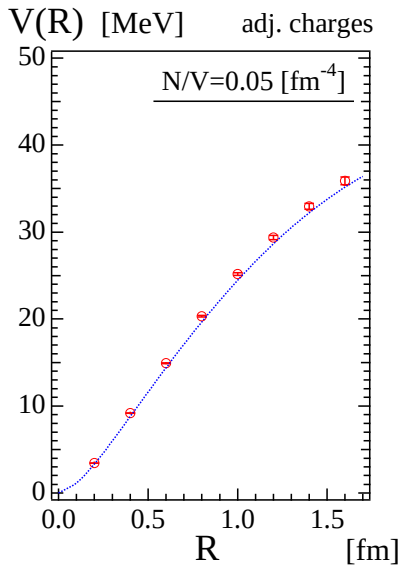

(a-ii)

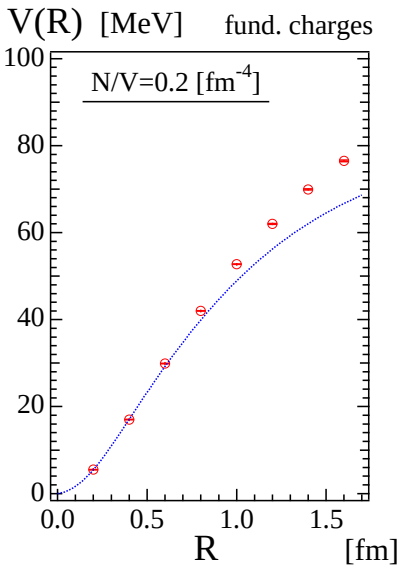

(b-i)

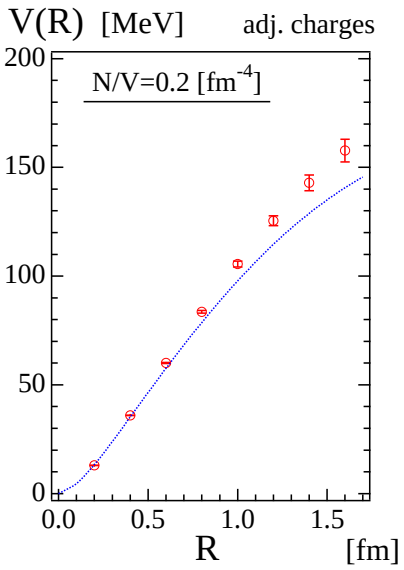

(b-ii)

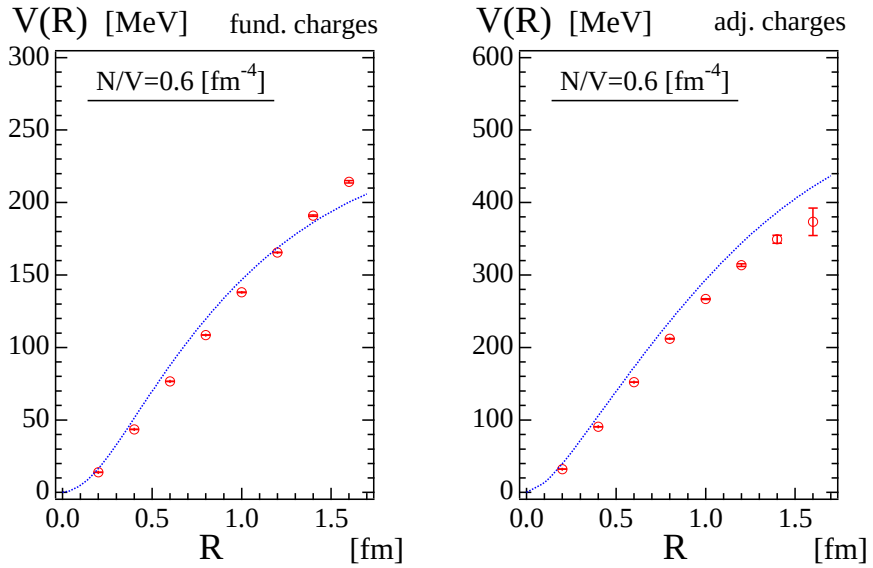

(c-i) (c-ii)

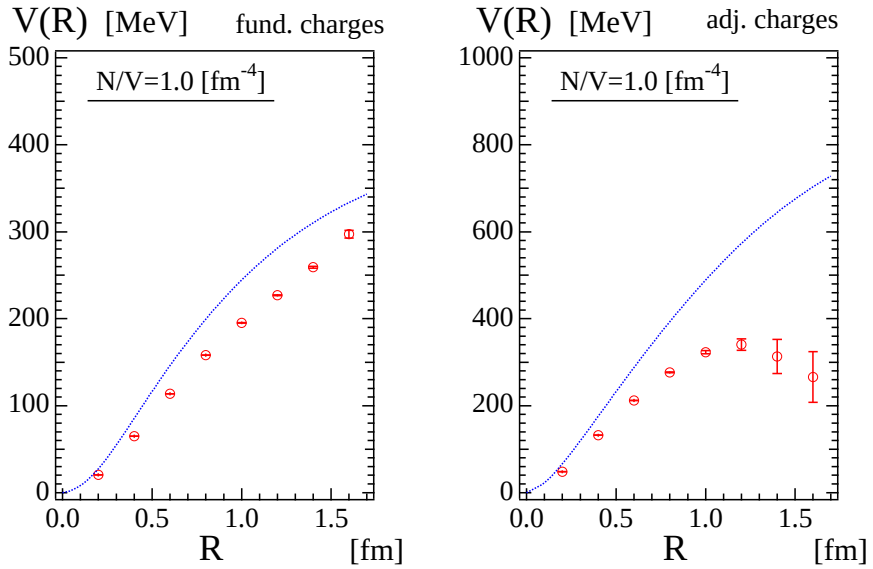

(d-i) (d-ii)

FIG. 1. The static non-Abelian potential derived from simulations of the random instanton liquid and from a dilute gas (one-instanton) approximation for fundamental (i) and adjoint (ii) charges The comparison is made for instanton densities $N/V = 0.05,\ 0.2,\ 0.6$ and 1.0 fm^{-4}. The curves describe the dilute gas approximation, the data points simulation results.

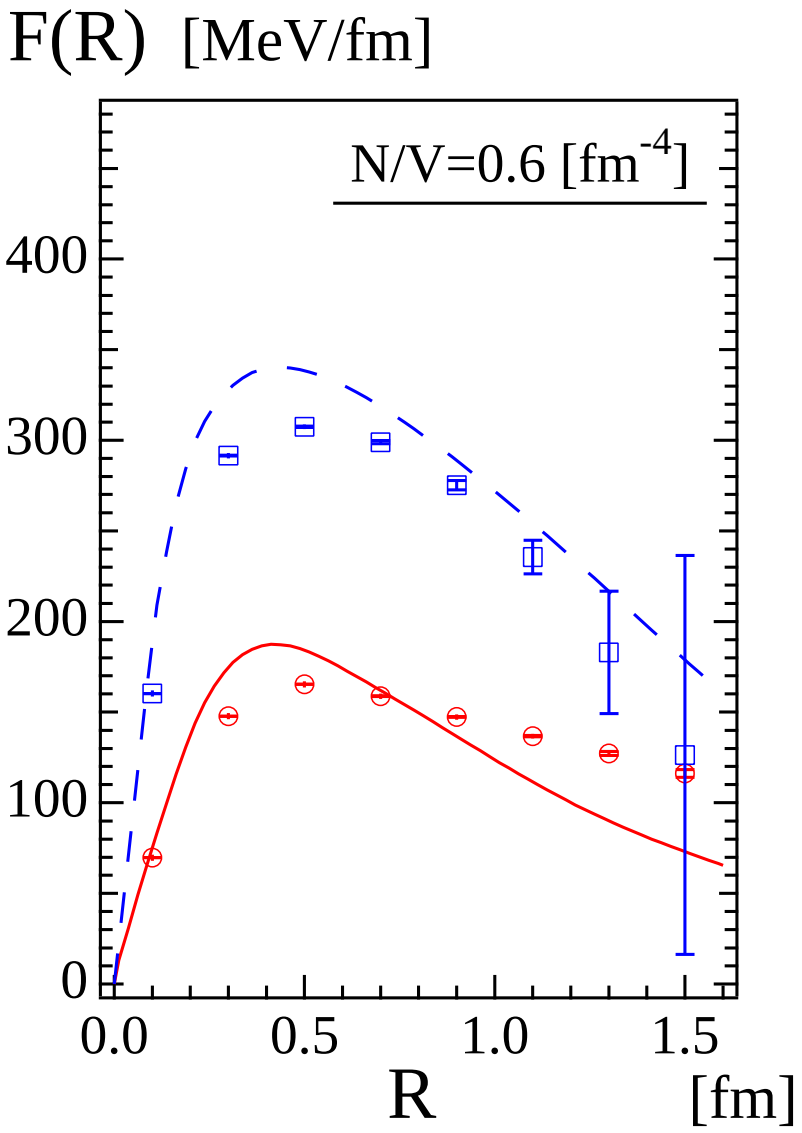

FIG. 2. The static non-Abelian force derived from simulations of the random instanton liquid and from a dilute gas (one-instanton) approximation for fundamental (circle) and adjoint (square) charges. The comparison is made for an instanton density $N/V = 0.6$ fm^{-4}. The curves and the dotted curves describe the dilute gas approximation for fundamental and adjoint charges, respectively.

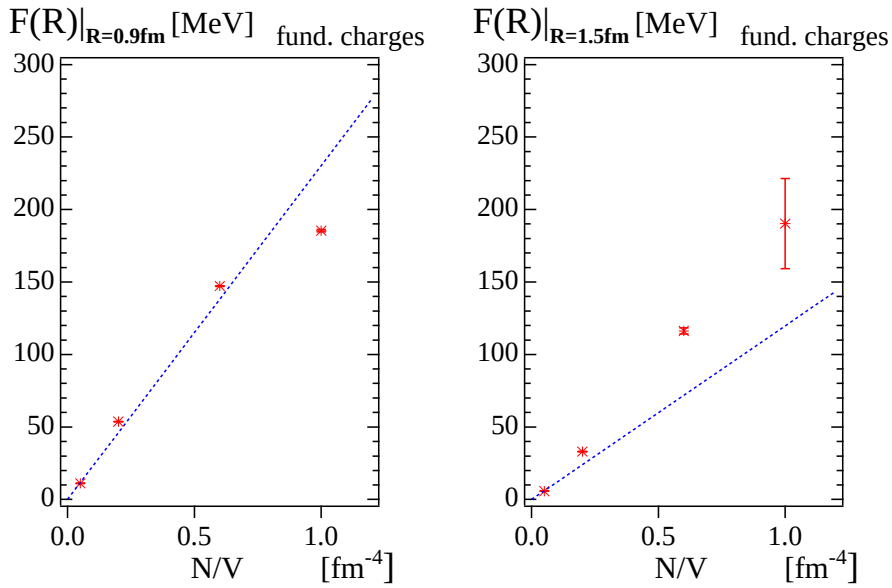

(a-i)

(a-ii)

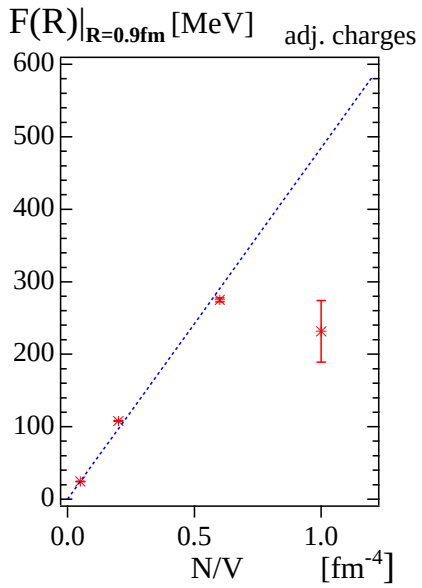

(b-i)

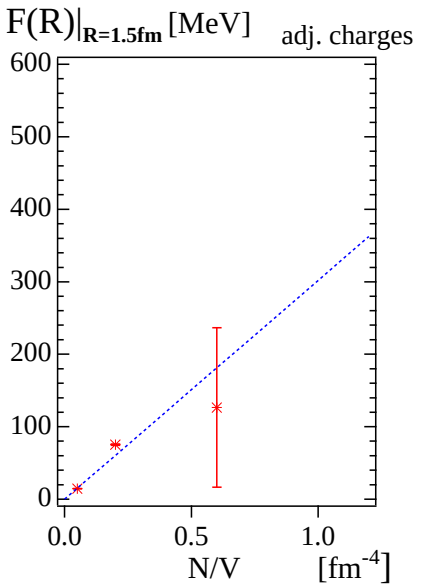

(b-ii)

FIG. 3. The density dependence of the forces at distance $R = 0.9$ fm and $R = 1.5$ fm for (a) fundamental and (b) adjoint charges. The solid curves describe the dilute gas approximation and the data points correspond to the simulation results.

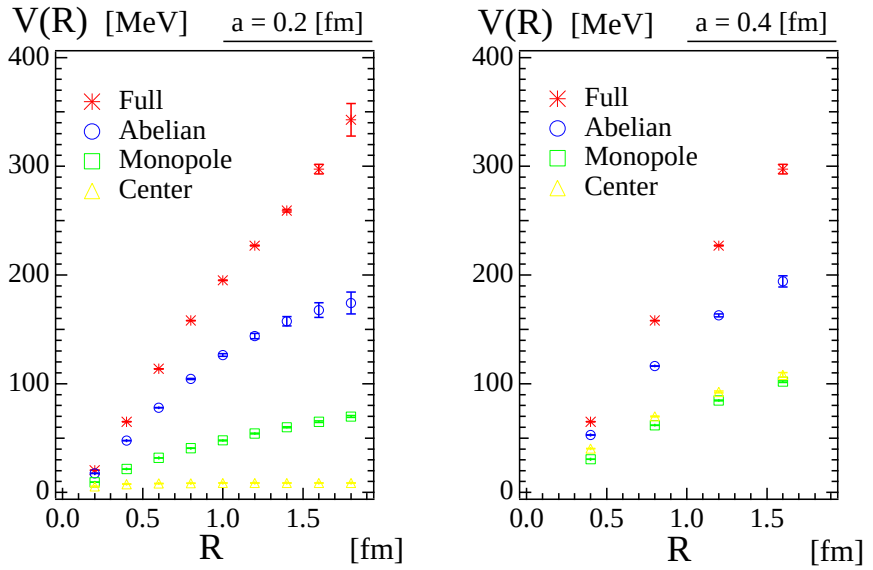

(a)

(b)

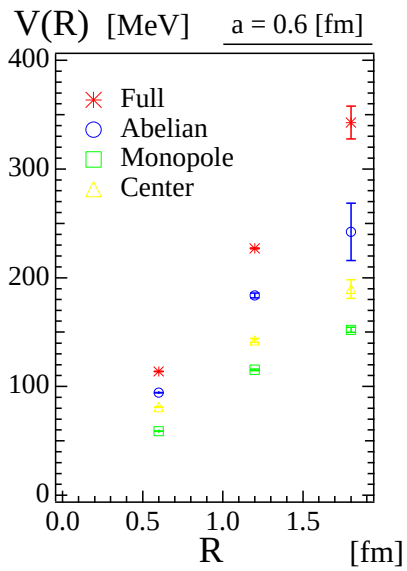

(c)

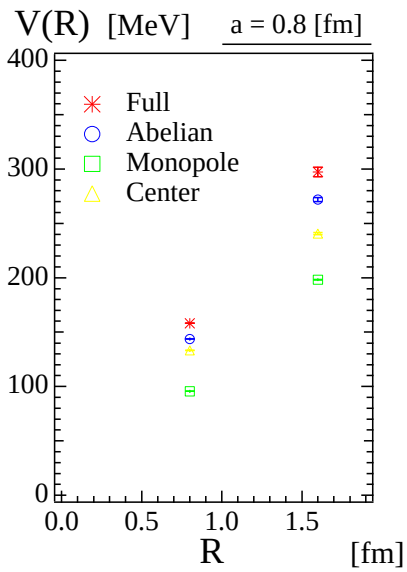

(d)

FIG. 4. The non-Abelian static potential of fundamental charges compared with the Abelian projection, its monopole component and with the potential in $Z(2)$ center projection, for different lattice spacings (a) $a = 0.20$ fm, (b) $a = 0.40$ fm, (c) $a = 0.60$ fm and (d) $a = 0.80$ fm. The instanton size and density is fixed to $\bar{\rho} = 0.4$ fm and $N/V = 1$ fm.

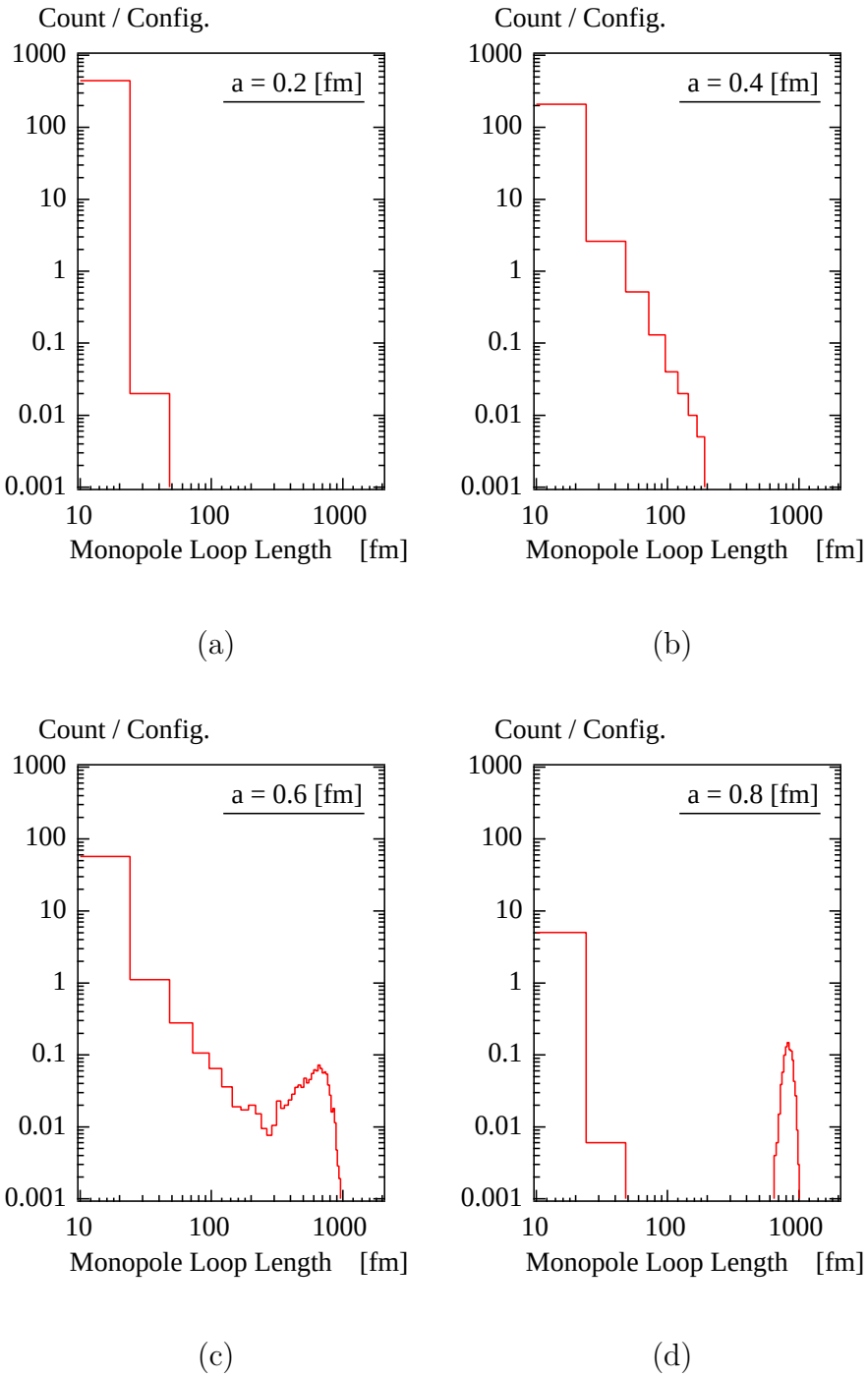

FIG. 5. Histograms of connected monopole clusters per configuration with respect to their lengths shown for different discretization scales (a) $a = 0.20$ fm (b) $a = 0.40$ fm, (c) $a = 0.60$ fm and (d) $a = 0.80$ fm.

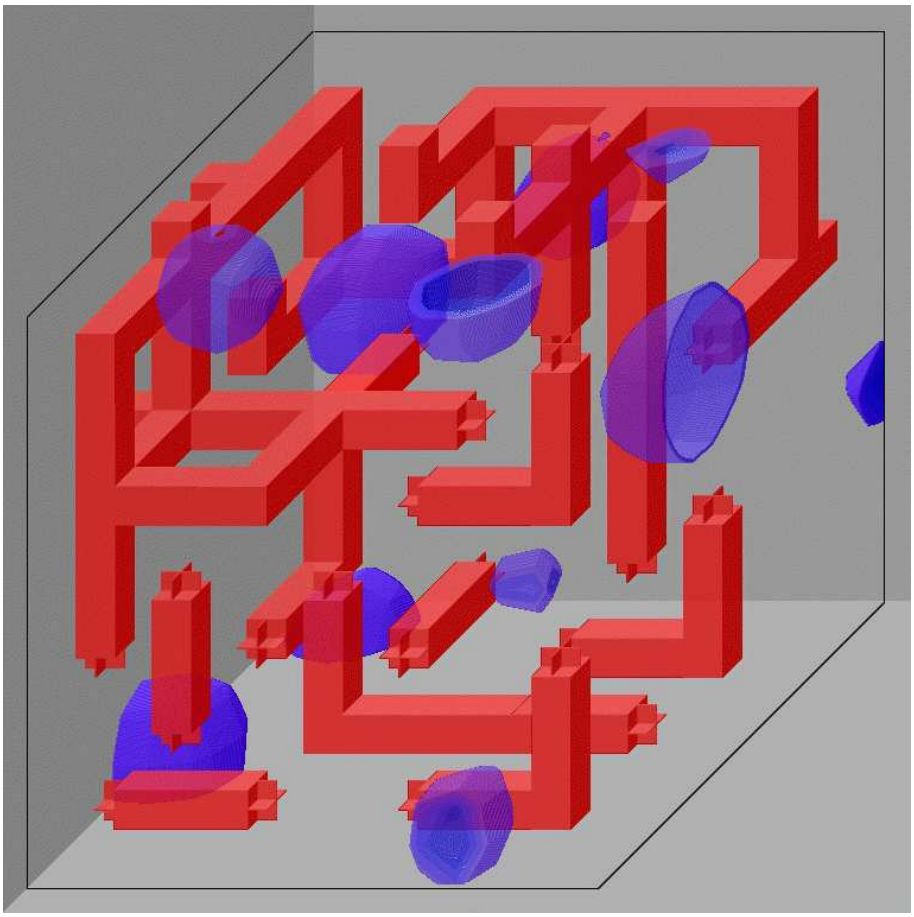

FIG. 6. Glance into a time-slice of a typical configuration with continuum instantons (balls) and lattice monopoles (bars) living on the coarsest lattice (with lattice spacing $a = 0.8$ fm). Only a subvolume $V = (3.2 \text{ fm})^3$ is shown.